



HAL
open science

Persistent Organic Room-Temperature Phosphorescence in Cyclohexane-trans-1,2- Bisphthalimide Derivatives: The Dramatic Impact of Heterochiral vs. Homochiral interactions

Ludovic Favereau, Cassandre Quinton, Cyril Poriel, Thierry Roisnel, Denis Jacquemin, Jeanne Crassous

► To cite this version:

Ludovic Favereau, Cassandre Quinton, Cyril Poriel, Thierry Roisnel, Denis Jacquemin, et al.. Persistent Organic Room-Temperature Phosphorescence in Cyclohexane-trans-1,2- Bisphthalimide Derivatives: The Dramatic Impact of Heterochiral vs. Homochiral interactions. *Journal of Physical Chemistry Letters*, 2020, 11 (15), pp.6426-6434. 10.1021/acs.jpcllett.0c01816 . hal-02999452

HAL Id: hal-02999452

<https://univ-rennes.hal.science/hal-02999452>

Submitted on 10 Nov 2020

HAL is a multi-disciplinary open access archive for the deposit and dissemination of scientific research documents, whether they are published or not. The documents may come from teaching and research institutions in France or abroad, or from public or private research centers.

L'archive ouverte pluridisciplinaire **HAL**, est destinée au dépôt et à la diffusion de documents scientifiques de niveau recherche, publiés ou non, émanant des établissements d'enseignement et de recherche français ou étrangers, des laboratoires publics ou privés.

Persistent Organic Room-Temperature Phosphorescence in Cyclohexane-*trans*-1,2-Bisphthalimide Derivatives: The Dramatic Impact of Heterochiral vs. Homochiral interactions

Ludovic Favereau,^{a,*} Cassandre Quinton,^a Cyril Poriel,^a Thierry Roisnel,^a Denis Jacquemin,^b Jeanne Crassous^a

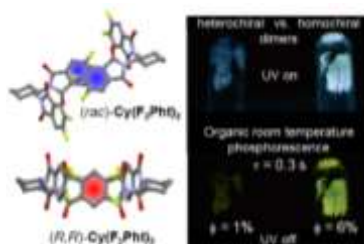
^a Univ Rennes, CNRS, ISCR-UMR 6226, ScanMAT-UMS 2001, F-35000 Rennes, France. E-mail: ludovic.favereau@univ-rennes1.fr

^b Laboratoire CEISAM, UMR 6230, CNRS, Université de Nantes, Nantes, France.

Abstract

Persistent metal-free Room-Temperature Phosphorescence (RTP) materials attract significant interest owing to the production of long-lived triplet excited states. Although several organic designs show RTP, the impact of intermolecular interactions on the triplet excitons stabilization and migrations remains hardly understood because obtaining different ordered intermolecular interactions while conserving identical molecular electronic properties is very challenging. We propose here a new strategy to circumvent this problem by taking advantage of the distinct molecular packing that can be found between enantiomer and racemic forms of a chiral molecule. Structural, photophysical and chiroptical investigations of chiral cyclohexane bisphthalimide derivatives showed that heterochiral and homochiral dimer interactions play a crucial role on the triplet excited state stabilization, resulting in higher RTP efficiency for enantiopure systems than for racemic one. This study paves the way to the use of molecular chirality to rationalize supramolecular properties arising from subtle intermolecular interactions.

TOC Graphic

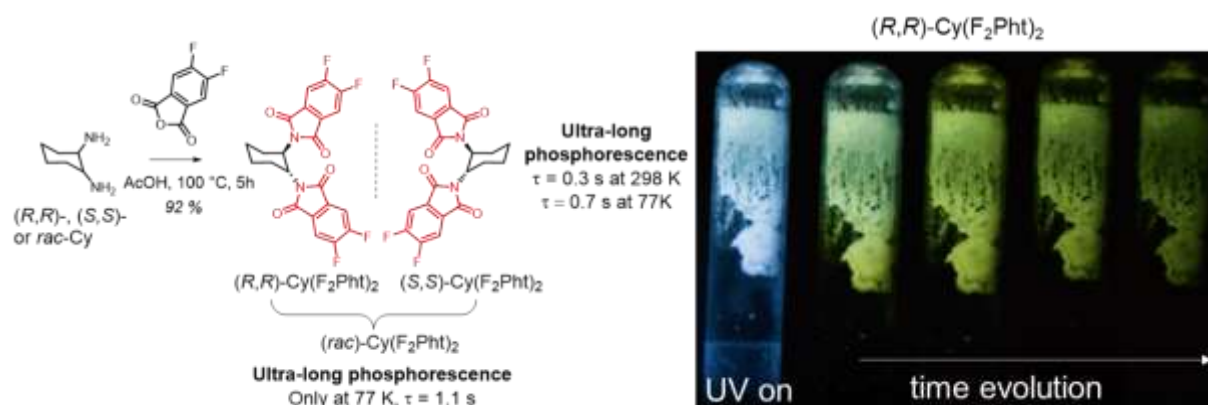


The organization of π -conjugated molecules in the solid state plays a pivotal role on the photophysical and electronic properties of the obtained material.^{1, 2, 3} Understanding the relationships between molecular structure, the intermolecular interactions and the resulting

properties of the supramolecular assembly is therefore of prime importance.⁴ Indeed, the arrangement of molecules within a material does strongly impact many nanoscale phenomena such as light absorption, luminescence, energy transfer, charges conduction or analyte sensing, which ultimately control the overall activity of the resulting macrostructure. In addition, supramolecular assemblies may yield emerging properties owing to specific molecular electronic interactions and organization. In this global framework, persistent metal-free Room-Temperature Phosphorescence (RTP) materials has attracted a growing interest owing to the production of long-lived triplet excited states, relevant for several applications, *e.g.*, optoelectronics (OPVs, OLEDs), bio-imaging, sensing, cryptography, photocatalysis.^{5, 6, 7, 8, 9, 10, 11} While phosphorescent metal-containing systems are well-known and rely on an efficient inter-system crossing (ISC) process induced by the large spin-orbit couplings (SOCs) of metal,^{12, 13} organic heavy-atom-free RTP materials have several advantages, such as lower cost and toxicity, and more tuneable photophysical properties.^{14, 15} In organic systems, RTP can typically take place by improving ISC efficiency, which can be done either by increasing the SOC using heavy halogen atoms such as bromine or iodide, or promoted by the presence of low-lying transitions following El-Sayed's rule. This can be achieved using heterocycles or carbonyl groups for instance.^{16, 17, 18} Besides these electronic factors, structural rigidity and ordered packing are also crucial parameters to minimize the radiationless deactivation of the ultra-long lived excited triplet states.^{19, 20, 21, 22, 23, 24, 25, 26, 27, 28} An effective understanding of the underlying photophysical process is needed to optimize the design of organic RTP molecular materials, and, more precisely, the impact of intermolecular interactions on the triplet exciton stabilization and migration needs to be understood. Such task is however made difficult, as obtaining different intermolecular interactions while keeping the same molecular electronic properties is often beyond reach, *e.g.*, the addition of methylene substituent in a lateral alkyl chain may induce a completely different solid state packing.^{25, 27} To circumvent this problem, chirality offers a unique possibility to investigate such parameters since enantiomer and racemic forms of a chiral molecule have identical chemical and physical properties in solution,²⁹ but may present distinct molecular packing as heterochiral and homochiral dimer interactions might differ, which in turn can yield different photophysical properties and/or electronic conduction.^{30, 31, 32, 33, 34, 35, 36} Accordingly, organic chiral compounds with RTP property modulated by enantiopurity represents an exceptional opportunity for exploring the impact of intermolecular interactions on the efficiency of ultra-long RTP without altering the molecular electronic properties. Moreover, the possibility to obtain RT circularly polarized luminescence (CPL) with chiral organic emitters could bring additional advantages over unpolarized RTP,³⁷

^{38,39} notably in the design of efficient CP-OLEDs, in spintronic, optical information processing, as well as in bioimaging (ellipsometry-based tomography) and chiral sensing, where the state of light polarization (either left or right) may bring higher contrast and selectivity than for a non-polarized light.

During our work on chiral π -conjugated molecules for chiroptoelectronic applications,^{30, 40, 41} we serendipitously noticed that enantiopure cyclohexane-*trans*-1,2-bisphthalimide derivatives, **(*RR*)-Cy(F₂Pht)₂**,⁴² display persistent RTP emission process once precipitated in the reaction medium. Irradiation of the obtained solid by UV light at $\lambda = 365$ nm (benchtop UV lamp) affords light blue luminescence, which evolves in a yellow one, seen by the naked eye upon switching off the excitation light (Scheme 1). This behaviour prompted us to explore the possible impact of molecular enantiopurity on the RTP efficiency. Herein we report our results regarding the study of chiral organic persistent RTP molecular materials based on cyclohexane tetrafluorinated derivatives (*(RR)*-, *(SS)*- and *(rac)*-**Cy(F₂Pht)₂**, Figure 1). Crystals of **Cy(F₂Pht)₂** display ultra-long yellow phosphorescence, which is dependent on both the enantiopurity of the molecular components and the temperature. While enantiopure and racemic crystals exhibit persistent phosphorescence at 77 K, only the former shows efficient RTP under ambient (air) conditions with a lifetime of 0.3 s. X-ray analysis, chiroptical, and photophysical characterizations reveal key differences in the stabilization of the triplet states within the different crystal arrangements of the enantiopure and racemic compounds. This study represents an unprecedented example of chiral persistent RTP materials in which enantiopurity controls the emission efficiency by modifying the crystal intermolecular packing of sterically and electronically identical individual components.



Scheme 1. Synthesis of (*RR*)-, (*SS*)- and (*rac*)-**Cy(F₂Pht)₂** with their main photophysical characteristics and picture of the RTP process for (*RR*)-**Cy(F₂Pht)₂**, under UV light excitation at $\lambda = 365$ nm (benchtop UV lamp) and after switched it off (time evolution).

(*RR*)-, (*SS*)- and (*rac*)-**Cy(F₂Pht)₂** were efficiently synthesized by mixing one equivalent of corresponding (*RR*)-, (*SS*)- or (*rac*)-cyclohexane-*trans*-1,2-diamine with excess of 5,6-difluoroisobenzofuran-1,3-dione in acetic acid in 92% yield for the three compounds (Scheme 1). These chiral derivatives were fully characterized by NMR, chiral HPLC and mass spectrometry,⁴² displaying characteristic signals of both phthalimide and cyclohexane units in the aromatic and aliphatic parts of the ¹H spectrum, respectively, with a C₂ symmetry for the bisphthalimide moieties (see the SI for details).^{43,44} Crystals of both (*RR*)- and (*rac*)-**Cy(F₂Pht)₂** have been obtained by slow diffusion of pentane vapours into chloroform solutions and their resulting X-ray structures show distinct features regarding the molecular geometry and the supramolecular arrangement: (*RR*)- and (*rac*)-**Cy(F₂Pht)₂** crystallize in the C222₁ and P $\bar{1}$ space group, respectively (Figure 1 and table S1), with the expected equatorial conformation for the phthalimide substituents attached to the cyclohexane backbone. While the two phthalimide planes form an angle of *ca.* 56° in the racemic compound, the enantiopure (*RR*)-**Cy(F₂Pht)₂** shows a more open structure with an angle of 71° (Figures 1a and 1b). In addition, different N1-C1-C2-N2 torsion angles are found in (*rac*)- and (*RR*)-**Cy(F₂Pht)₂**: 49.3° and 60.6°, respectively, resulting in a less face-to-face phthalimides arrangement for the former. These significant differences may be attributed to symmetry reasons, which sometimes induce different packing between pure enantiomers and corresponding racemic mixture.²⁹ While (*rac*)- and (*RR*)-**Cy(F₂Pht)₂** form similar phthalimide dimers in a head-to-tail fashion, separated by 3.46 and 3.53 Å, respectively (Figures 1c and 1d), expanding the packing to the supramolecular level reveals important differences between both crystals. Indeed, (*RR*)-**Cy(F₂Pht)₂** dimers exhibit a continuous intermolecular chain along the x axis, maintained by identical π - π interactions involving each phthalimide unit (Figure 1f), whereas (*rac*)-**Cy(F₂Pht)₂** dimers present π - π intermolecular interactions along the y axis with other dimer neighbours (blue colour, Figure 1e). In this additional dimer interaction, the phthalimide groups are separated by 3.45 Å and appear much less co-facially oriented than the previously described red one, affording distinct molecular arrangements for homo- and heterochiral dimer interactions. Further single-crystal X-ray diffraction analysis show that for the red dimers, the angle between transition dipoles and the interconnected axis is larger than the critical value of 54.7° ($\theta = 71.5$ and 77.6° for (*rac*)- and (*RR*)-**Cy(F₂Pht)₂**, respectively, Figure 1c,d), indicating the presence of H-aggregates (see the SI for details), while for the blue dimer, this angle is around 55.4° at the boarder between H- and J-aggregates states.^{16, 45, 46} Fluorine atoms might have an indirect effect on the overserved solid-state arrangement since in the crystal structure, one fluorine atom

shows a short contact bond with an aromatic proton of a phthalimide fragment neighbors for (RR) - $\text{Cy}(\text{F}_2\text{Pht})_2$ or with an alkyl proton of the cyclohexane core in the case of rac - $\text{Cy}(\text{F}_2\text{Pht})_2$ (Figure 1), suggesting an effect on the molecular packing .

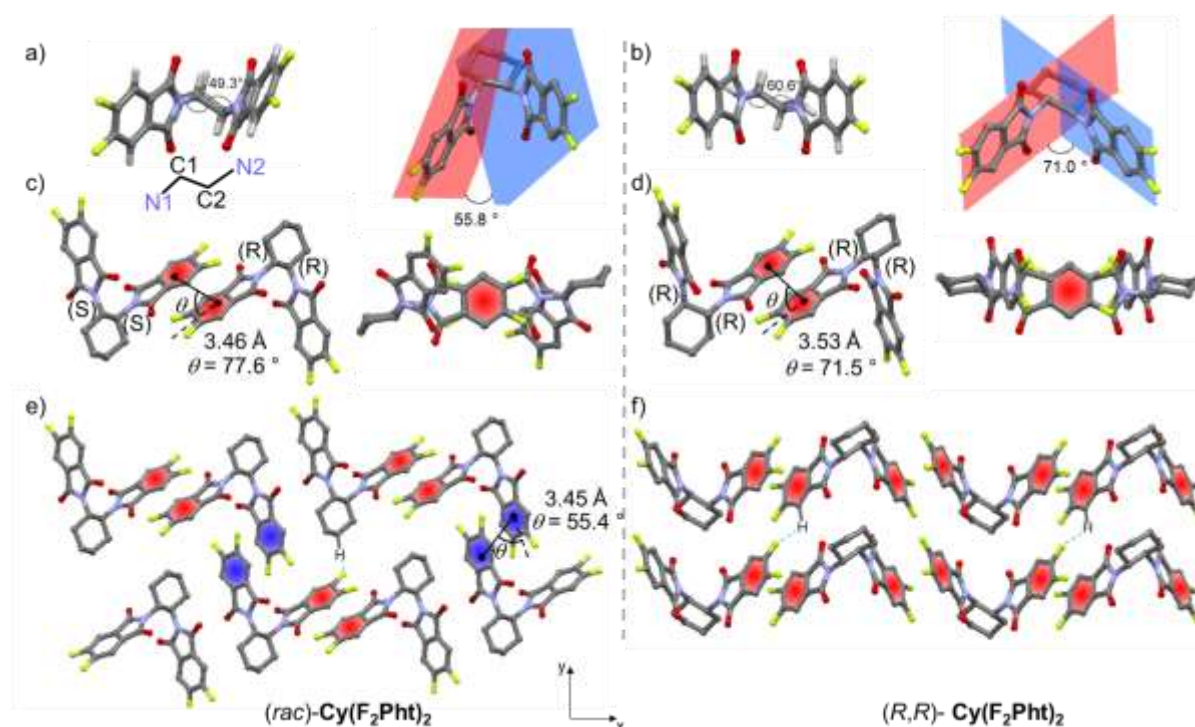


Figure 1. Comparison of the X-ray crystallographic structures of (rac) - $\text{Cy}(\text{F}_2\text{Pht})_2$ (left, a) and (RR) - $\text{Cy}(\text{F}_2\text{Pht})_2$ (right, b) at the molecular level with N1-C1-C2-N2 dihedral angle and angle between phthalimide plans; and at the supramolecular level with different views of intermolecular interactions between dimers, c) and d); and supramolecular packing e) and f). θ angles represent the angle between the transition dipoles and interconnected axis of (rac) - $\text{Cy}(\text{F}_2\text{Pht})_2$ and (RR) - $\text{Cy}(\text{F}_2\text{Pht})_2$ with values of 71.5° and 77.6° , respectively for the red dimers, evidencing the presence of H aggregates, in comparison to the blue dimer ($\theta = 55.4^\circ$, see SI for additional details).

The UV-vis spectrum of $\text{Cy}(\text{F}_2\text{Pht})_2$ in dilute solution (10^{-5} M) displays an intense absorption bands at ca. 230 nm ($\epsilon = 5.5 \times 10^4 \text{ M}^{-1}\text{cm}^{-1}$) and smaller broader one at 285 nm ($\epsilon = 2.0 \times 10^3 \text{ M}^{-1}\text{cm}^{-1}$), respectively assigned to π - π^* and n - π^* transitions (Figure 2).⁴³ At 298 K in dichloromethane solution, $\text{Cy}(\text{F}_2\text{Pht})_2$ exhibits a very weak luminescence at ca. 310 nm ($\phi < 0.01$), presumably due to an efficient ISC process from the singlet to the triplet excited state of the molecule, as already reported for phthalimide derivatives.⁴⁷ Indeed, lowering the temperature to 77 K affords a residual fluorescence signal at 300 nm and mainly phosphorescence emission, with a maximum at 461 nm and a lifetime of ca. 1 s arising from π -

π^* triplet state, in line with the phosphorescence emission reported for phthalimide derivatives (Figures 2 and S9). To gain further details, theoretical calculations were performed on **Cy(F₂Pht)₂** (see the SI). Upon light excitation, population of excited **Cy(F₂Pht)₂** singlet states (S_n) occurs, followed by internal conversion and relaxation to the lowest excited singlet state (S_1 , Figure 2). From the latter, a residual fluorescence emission occurs experimentally recorded at 312 nm, which is well reproduced by the calculations (319 nm, Figure 2). This radiative deactivation process is in competition with the ISC process leading to **Cy(F₂Pht)₂** triplet excited states. Theoretical calculations indicate the presence of eight triplet states close to S_1 in energy, with moderate to rather strong spin orbit coupling with values up to 4.3 and 4.6 cm^{-1} for the $S_1 \rightarrow T_6$ and $S_1 \rightarrow T_5$ transitions. These SOC are of significant intensity for organic systems without heavy atom and highlight the potential of this molecular system to investigate phosphorescence emission, which was also well reproduced by theoretical calculation at 447 nm (Figure 2). For comparison purpose, mono phthalimide derivative **CyF₂Pht** was also synthesized and its optical properties characterized. **CyF₂Pht** displays almost the same UV-vis absorption and luminescence profiles than those of **Cy(F₂Pht)₂**, notably a similar low temperature phosphorescence emission at 460 nm with a lifetime of *ca.* 0.8 s. These results suggest a weak electronic interaction between the two phthalimide units in **Cy(F₂Pht)₂**, consistent with their arrangements (see Figure 1) and with its molar extinction coefficients twice as high as for **CyF₂Pht**. As expected, the cyclohexane-trans-1,2-bisamido linker has a limited role of in term of photophysics due to its sp^3 core but remains crucial as it brings the property of chirality owing to the presence of the two enantiomers (*RR* and *SS*) for this conformation.

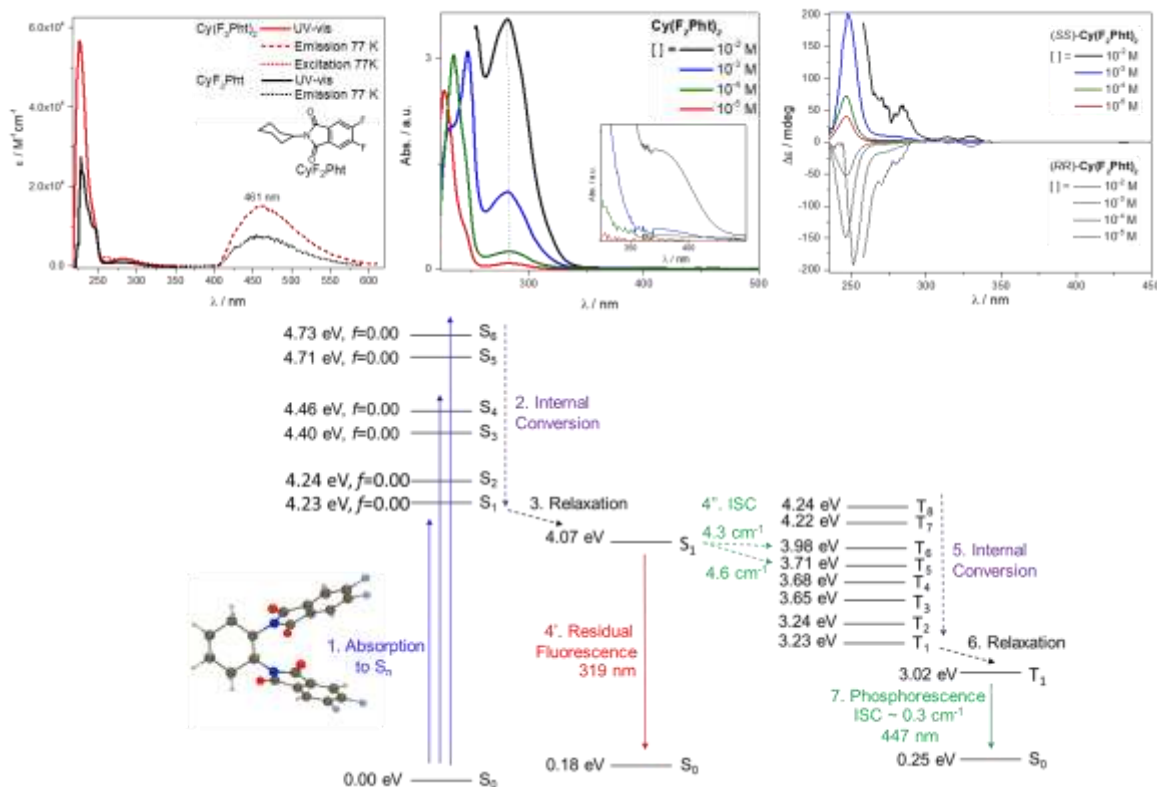


Figure 2. Top: left: UV-vis absorption spectrum of $Cy(F_2Pht)_2$ and CyF_2Pht in dichloromethane solution ($\sim 10^{-5}$ M, red and black, respectively) at 298 K together with their emission spectrum recorded in 2-MeTHF at 77 K (red and black dashed lines, respectively, $\lambda_{exci} = 280$ nm) and the corresponding excitation spectrum of $Cy(F_2Pht)_2$ (red dotted line, $\lambda_{exci} = 460$ nm); middle: UV-vis absorption spectra of $Cy(F_2Pht)_2$ recorded at different concentration: 10^{-5} (red), 10^{-4} (green), 10^{-3} (blue) and 10^{-2} M (black) in dichloromethane solution at 298 K; right: Electronic Circular Dichroism spectra of (RR)- and (SS)- $Cy(F_2Pht)_2$ recorded at different concentration: 10^{-5} (red), 10^{-4} (green), 10^{-3} (blue) and 10^{-2} M (black) in dichloromethane solution at 298 K (due to rapid signal saturation upon increasing concentration, only the 230-450 nm region is displayed). Bottom: Energy-level diagrams and calculated ISC channels from the ground state S_0 to the singlet excited states (S_n) and finally the triplet excited states (T_n) with the most significant corresponding spin-orbit coupling (SOC) constants.

Further insights have been obtained by recording the Electronic Circular Dichroism (ECD) of (RR)- and (SS)- $Cy(F_2Pht)_2$ (Figure S7), which exhibited the expected mirror-image spectra with positive intense bands at 230 and 242 nm ($\Delta\epsilon \sim 35$ $M^{-1}cm^{-1}$), arising from two chiral excitonic couplings between the perpendicular in-plane electronic dipoles present in each phthalimide unit,⁴³ and an additional very weak transition around 280 nm for (SS)- $Cy(F_2Pht)_2$

($\Delta\epsilon \sim -0.5 \text{ M}^{-1}\text{cm}^{-1}$). Increasing solution concentrations up to 10^{-2} M does not induce drastic changes in the UV-vis signature and mainly resulted in a small 15 nm red-shift of the band at 230 nm, a proportional intensity increase of the n- π^* transitions absorption at ca. 285 nm with a slight blue-shift of 3 nm, and the apparition of a weak band between 340 and 400 nm when the concentration attains 10^{-3} - 10^{-2} M (Figure 2), suggesting the presence of intermolecular interactions. Likewise, ECD of concentrated solutions reveals the appearance of very weak mirror-image signals up to 350 nm, marked by two positive maxima at 315 and 330 nm for (SS)-**Cy(F₂Pht)₂** (Figure 2), while the rest of the ECD spectrum becomes above the detection range of the detector. The obtained X-ray crystallographic structures and the slight blue-shift of the absorption spectra upon increasing concentration are consistent with a predominant contribution of H-aggregates between intermolecular phthalimide fragments, which have been identified as an important parameter for stabilization of triplet excitons and RTP in organic systems.^{14, 15, 17, 21} Similar experiments on monophthalimide model compound, **CyF₂Pht**, gives identical optical signature for concentrated solution (Figures S13-S15), which confirms the involvement of intermolecular interactions. Such aggregation behaviour also modifies the luminescence properties of **Cy(F₂Pht)₂** since the emission spectra display significant changes at high concentration including a decrease of the low emissive band around 310 nm (Figure 3a), concomitantly with the appearance of weakly luminescence around 420 nm, presumably arising from H-type dimers. Indeed, excitation of the sample at 360 nm, *i.e.*, in the absorption band attributed to intermolecular interactions, results in similar fluorescence emission at 425 nm ($\tau = 2.2$ and 12 ns, Figure 3b). Moreover, excitation spectra at 425 nm clearly indicate that this emission band involved molecular and intermolecular optical transitions at 260-280 nm and between 340 and 400 nm, respectively (Figure S8). Overall, these photophysical characterizations in solution show the tendency of **Cy(F₂Pht)₂** to form weakly fluorescent aggregates at high concentration, as expected for H-type molecular interactions,⁴⁸ but do not afford any evidence of phosphorescence emission, nor of different signatures of the racemic and enantiopure supramolecular assemblies.

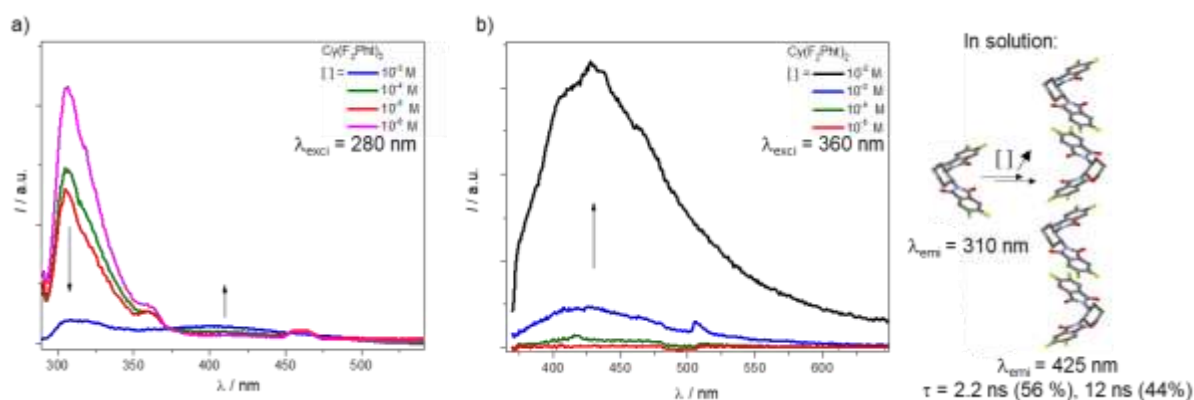


Figure 3. a) Luminescence spectra of **Cy(F₂Pht)₂** recorded at different concentrations: 10⁻⁶ (purple), 10⁻⁵ (red), 10⁻⁴ (green) and 10⁻³ M (blue) in dichloromethane solution at 298 K ($\lambda_{\text{exci}} = 280$ nm); b) luminescence spectra of **Cy(F₂Pht)₂** recorded at different concentration: 10⁻⁵ (red), 10⁻⁴ (green), 10⁻³ (blue) and 10⁻² M (black) in dichloromethane solution at 298 K ($\lambda_{\text{exci}} = 360$ nm) with illustration of the presumably molecular aggregation in highly concentrated solutions.

The luminescence properties of the (*RR*)-, (*SS*)-, (*rac*)-**Cy(F₂Pht)₂** crystals are displayed in Figure 4. At 298 K in air atmosphere, (*rac*)-**Cy(F₂Pht)₂** crystals excited at 330 nm give a weak and broad emission spectrum with two hardly distinguishable and similarly intense bands at 435 and 530 nm. When excitation takes place at 350 nm, a similar luminescence profile is observed but with a slightly higher emission intensity for the 435 nm emission band. Such change becomes clearer when the crystals are excited at 370 nm, corresponding to the intermolecular interactions from the phthalimide aggregates, since the signal at 530 nm appears only as a shoulder of the main emission process at 435 nm. In comparison, while excitation of (*RR*)-**Cy(F₂Pht)₂** crystals at 370 nm affords a similar emission spectrum with a maximum at 440 nm, the excitations at 330 and 350 nm result in different luminescence profiles. Indeed, upon excitation at 350 nm, (*RR*)-**Cy(F₂Pht)₂** displays two well resolved emission bands at 440 and 525 nm, the latter being of higher intensity, which strikingly differ from (*rac*)-**Cy(F₂Pht)₂**. Finally, the predominance of the emission process at 525 nm is even more pronounced when the enantiopure crystals are excited at 330 nm (I^{530}/I^{425} ratio of 14). Importantly, yellow RTP remains clearly present after switching off the excitation source at all these excitation wavelengths, suggesting that this process may be related to the emission band at 530 nm. Indeed, emission spectra of (*RR*)-**Cy(F₂Pht)₂** crystals excited at 350 nm and recorded after 10, 30 and 50 ms of delay afford an identical vibronic responses with maxima at 496 and 532 nm. To gain further insights, time-resolved luminescence measurements have been recorded at these two luminescence maxima. At 530 nm, a very long lifetime (τ) of ~ 0.3 s was detected as the

main decay component for the RTP process whereas at 435 nm, only a short nanosecond lifetime was recorded (Figure S9). Such measurements allowed us to assign the two observed emission bands at 435 and 530 nm to singlet (S_1) and triplet (T_1) emissions of the (*RR*)-**Cy(F₂Pht)₂** aggregates, since the former is close to the fluorescence observed in concentrated solution (Figure 3) whereas the phosphorescence at 530 nm appears redshifted as compared to the molecular phosphorescence recorded in frozen solution of diluted **Cy(F₂Pht)₂** at 77 K (Figure 2).

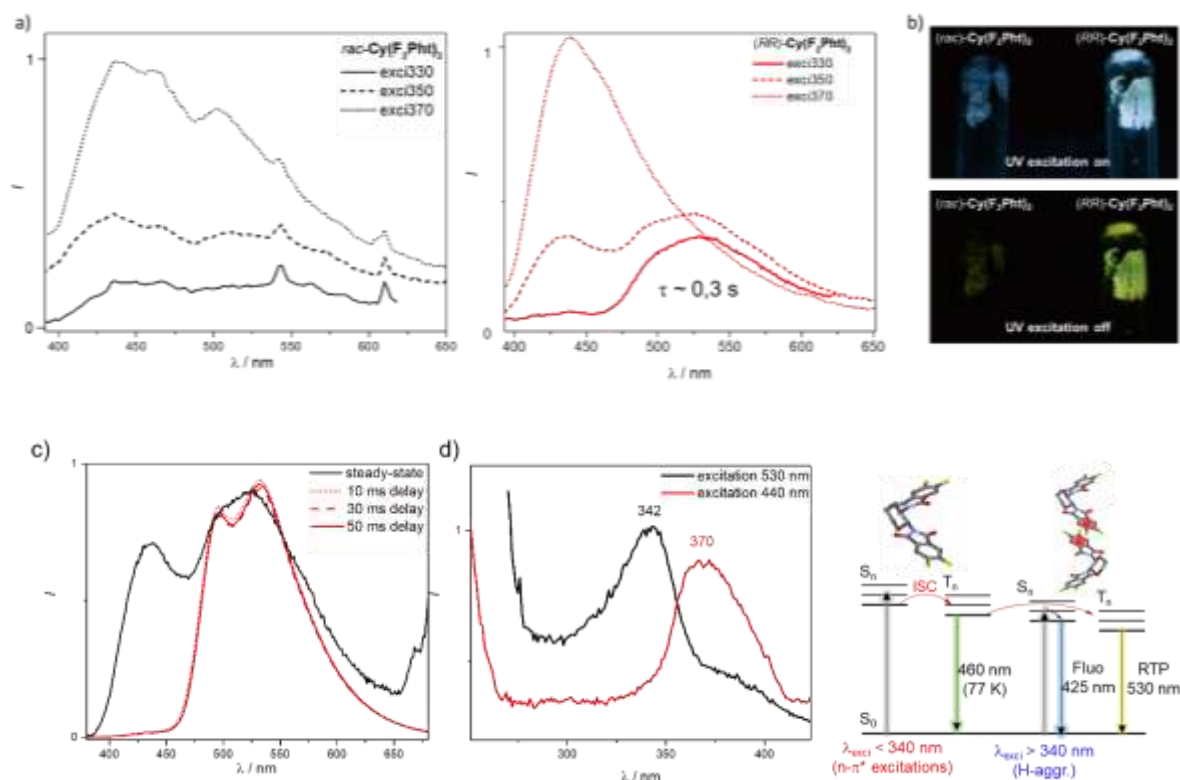


Figure 4. a) Luminescence spectra of (*rac*)-**Cy(F₂Pht)₂** crystals (left, black lines) and (*RR*)-**Cy(F₂Pht)₂** (right, red lines) recorded at different wavelength excitations: 330 (solid line), 350 (dashed line) and 370 nm (dotted line) at 298 K; b) top: pictures showing luminescence of (*rac*)-**Cy(F₂Pht)₂** (left) and (*RR*)-**Cy(F₂Pht)₂** (right) under UV light excitation with benchtop UV lamp and bottom: just after switched it off; c) steady-state (black solid line) and delayed emission spectra (red lines, $\lambda_{\text{exci}} = 280$ nm), recorded at different times delays: 50 ms (solid line), 30 ms (dashed line) and 10 ms (dotted line) at 298 K; d) left: excitation of luminescence of (*RR*)-**Cy(F₂Pht)** recorded at 440 (red) and 525 nm (black) and right: proposed mechanism of RTP generation with impact of excitation wavelengths.

We have also investigated the luminescence excitation spectra at 440 and 525 nm. The latter notably indicated that the electronic transitions responsible for the fluorescence and

phosphorescence emissions involve different absorption bands, which may be assigned to intermolecular aggregates (350 – 410 nm) and molecular absorption bands ($\lambda < 350$ nm), respectively (Figure 4 c), and suggest that the observed RTP process is more efficiently triggered when light excitations occurs on electronic transitions of the molecular unit (for $\lambda_{exc} < 350$ nm). According to photophysical studies of phthalimides,^{43, 47} the lower part of their absorption spectrum (280-340 nm) is dominated by $n-\pi^*$ electronic transitions, which are associated to a high ISC rate between the singlet $^1(n-\pi^*)$ and lowest triplet $^3(\pi,\pi^*)$ excited states in accordance with El-Sayed's rule,⁴⁹ and as evidenced here by the recorded phosphorescence process in diluted phthalimide solution at 77 K. Such fast ISC process should occur in both racemic and enantiopure crystals of **Cy(F₂Pht)₂** when exciting the molecular electronic transitions ($\lambda_{exc} < 350$ nm). However, when one excites the absorption band related to the intermolecular aggregates, that is, for $\lambda_{exc} > 350$ nm, the ISC rate drops and fluorescence becomes the main radiative deactivation process. Interestingly, the racemic and enantiopure crystals did not emit with the same intensity, as can be seen in Figure 4. To ascertain such difference, a similar photophysical study was performed on (*SS*)-**Cy(F₂Pht)₂** and afforded, as expected, similar results as (*RR*)-**Cy(F₂Pht)₂** (see the SI for detail). Further, quantitative evidences of the impact of enantiopurity on the RTP efficiency were provided by luminescence quantum yield measurements recorded at different wavelengths. Both enantiopure crystals show close emission efficiencies with significant values of 2-3 and 3-6% when exciting either at 350 or 370 nm, respectively, while low quantum yields of 0.5 and 1% were measured for (*rac*)-**Cy(F₂Pht)₂** at 350 or 370 nm respectively, unambiguously reflecting the more efficient RTP process in enantiopure crystal. This fact is also confirmed by naked eyes since the yellow RTP is less bright and shorter than the one observed from enantiopure crystals (see videos in the SI).

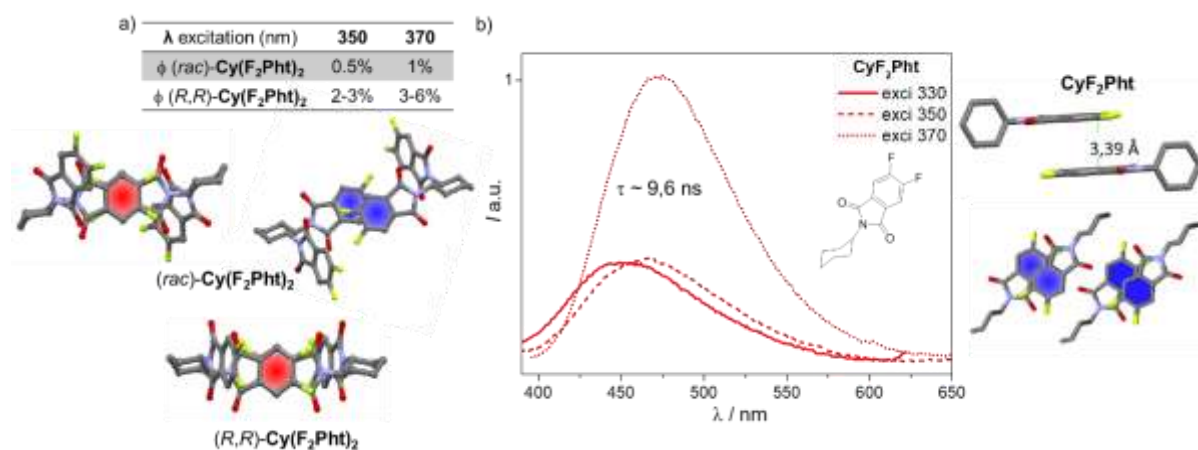


Figure 5. a) Luminescence quantum yields of (*RR*)-**Cy(F₂Pht)₂** and (*rac*)-**Cy(F₂Pht)₂** crystals recorded at 350 and 370 nm at 298 K; b) Luminescence spectra of **CyF₂Pht** crystals recorded at different wavelength excitations: 310 (solid line), 350 (dashed line) and 370 nm (dotted line) at 298 K with X-ray crystallographic structures of intermolecular dimers.

Since the photophysical experiments were performed on crystals, the RTP process can be directly related to the presence of the illustrated intermolecular red dimers of phthalimide fragments in Figure 1. As mentioned above, these dimers show characteristics of H-type aggregates, which have been identified as a stabilization strategy for triplet excitons and an efficient approach to get RTP in organic systems.^{16, 20, 21} Indeed, photophysical experiments performed on crystals of model compound **CyF₂Pht** did not reveal any RTP process, which could be explained by the lack of “red” H-aggregates found in **Cy(F₂Pht)₂** (Figure 5). Accordingly, the higher RTP efficiency in enantiopure **Cy(F₂Pht)₂** can be explained by the greater presence of such interactions in comparison with (*rac*)-**Cy(F₂Pht)₂**, highlighting the subtle and crucial role of the heterochiral and homochiral dimer interactions, ultimately leading to distinct molecular packing, and thus different RTP efficiency. Indeed, the presence of additional “blue” dimers for (*rac*)-**Cy(F₂Pht)₂** result in less H-type aggregates and a less ordered molecular network, which presumably decreases the stabilization of triplet excitons, as for **CyF₂Pht**. Such parameter was tentatively investigated by carrying out some photophysical experiments at 77 K to probe the impact of temperature on the stabilization of the phosphorescence arising from the supramolecular assembly (Figure S11-S12). Reducing the temperature clearly stabilizes and enhances the long emission process over the fluorescence one for both (*rac*)-**Cy(F₂Pht)₂** and (*RR*)-**Cy(F₂Pht)₂**, which exhibited phosphorescence at 490 nm with a lifetime of 1.1 and 0.7 s., respectively. When light excitation is performed at 350 nm, only weak fluorescence is observed for (*rac*)-**Cy(F₂Pht)₂** at 400 nm, indicating a critical role of the temperature on the deactivation of the triplet excited state for such derivative. Unfortunately, no circularly polarized RTP was observed from enantiopure crystals despite several attempts, presumably due to the low value of polarized emission in these derivatives.

We have reported RTP process in chiral metal free tetrafluorinated cyclohexane-*trans*-1,2-naphthalimide derivatives whose efficiency is modulated by the enantiopurity of the molecular component. This surprising aspect was assigned to a different organization of homo- and heterochiral dimers in the solid state, which has a crucial impact on the presence of H-type aggregates within the crystal network, as unambiguously ascertained by X-ray analysis. Such

symmetry parameter results in an efficient RTP for enantiopure crystal of **Cy(F₂Pht)₂** with a quantum yield of 3% and a lifetime of 0.3 s while, in contrast, (*rac*)-**Cy(F₂Pht)₂** displays a quantum yield of 0.5% only under ambient (air) conditions. Photophysical and chiroptical measurements afforded further insights on the structural parameters that stabilized triplet excitons within these chiral molecular networks and notably the crucial impact of intermolecular H-aggregates and temperature. These findings clearly highlight an interesting feature of chiral molecular materials on the modulation of supramolecular material properties by the degree of enantiopurity. It is our hope that these results may help in designing more efficient chiral RTP materials in order to obtain circularly polarized phosphorescence in metal free compounds.

Acknowledgments

We acknowledge the Ministère de l'Éducation Nationale, de la Recherche et de la Technologie, the Centre National de la Recherche Scientifique (CNRS). The PRISM core facility (Biogenouest©, UMS Biosit, Université de Rennes 1 - Campus de Villejean - 35043 RENNES Cedex, FRANCE) is acknowledged for the ECD measurements. The authors thanked Dr. N. Vanthuyne for the chiral HPLC analysis. Guillaume Juin is warmly thanked for his movie on the room temperature process.

Supporting Information

Additional detailed experimental information, synthesis, and graphs can be find in the Electronic Supporting Information.

References

1. Riera-Galindo, S.; Tamayo, A.; Mas-Torrent, M., Role of Polymorphism and Thin-Film Morphology in Organic Semiconductors Processed by Solution Shearing. *ACS Omega* **2018**, *3* (2), 2329-2339.
2. Ostroverkhova, O., Organic Optoelectronic Materials: Mechanisms and Applications. *Chem. Rev.* **2016**.
3. Beaujuge, P. M.; Fréchet, J. M. J., Molecular Design and Ordering Effects in π -Functional Materials for Transistor and Solar Cell Applications. *J. Am. Chem. Soc.* **2011**, *133* (50), 20009-20029.
4. Aida, T.; Meijer, E. W., Supramolecular Polymers – we've Come Full Circle. *Isr. J. Chem.* **2020**, *60* (1-2), 33-47.
5. Hirata, S.; Totani, K.; Zhang, J.; Yamashita, T.; Kaji, H.; Marder, S. R.; Watanabe, T.; Adachi, C., Efficient Persistent Room Temperature Phosphorescence in Organic Amorphous Materials under Ambient Conditions. *Adv. Funct. Mater.* **2013**, *23* (27), 3386-3397.

6. Mukherjee, S.; Thilagar, P., Recent advances in purely organic phosphorescent materials. *Chem. Commun.* **2015**, 51 (55), 10988-11003.
7. Ma, H.; Lv, A.; Fu, L.; Wang, S.; An, Z.; Shi, H.; Huang, W., Room-Temperature Phosphorescence in Metal-Free Organic Materials. *Annalen der Physik* **2019**, 531 (7), 1800482.
8. Chen, H.; Yao, X.; Ma, X.; Tian, H., Amorphous, Efficient, Room-Temperature Phosphorescent Metal-Free Polymers and Their Applications as Encryption Ink. *Adv. Opt. Mater.* **2016**, 4 (9), 1397-1401.
9. Wang, J.; Liang, J.; Xu, Y.; Liang, B.; Wei, J.; Li, C.; Mu, X.; Ye, K.; Wang, Y., Purely Organic Phosphorescence Emitter-Based Efficient Electroluminescence Devices. *J. Phys. Chem. Lett.* **2019**, 10 (19), 5983-5988.
10. Zhang, T.; Ma, X.; Wu, H.; Zhu, L.; Zhao, Y.; Tian, H., Molecular Engineering for Metal-Free Amorphous Materials with Room-Temperature Phosphorescence. *Angew. Chem. Int. Ed. Engl.* **2020**, 59 (28), 11206-11216.
11. Kabe, R.; Adachi, C., Organic long persistent luminescence. *Nature* **2017**, 550 (7676), 384-387.
12. Xu, H.; Chen, R.; Sun, Q.; Lai, W.; Su, Q.; Huang, W.; Liu, X., Recent progress in metal-organic complexes for optoelectronic applications. *Chem. Soc. Rev.* **2014**, 43 (10), 3259-3302.
13. Henwood, A. F.; Zysman-Colman, E., Lessons learned in tuning the optoelectronic properties of phosphorescent iridium(iii) complexes. *Chem. Commun.* **2016**.
14. Data, P.; Takeda, Y., Recent Advancements in and the Future of Organic Emitters: TADF- and RTP-Active Multifunctional Organic Materials. *Chem. Asian J.* **2019**, 14 (10), 1613-1636.
15. Kenry; Chen, C.; Liu, B., Enhancing the performance of pure organic room-temperature phosphorescent luminophores. *Nat. Commun.* **2019**, 10 (1), 2111.
16. An, Z.; Zheng, C.; Tao, Y.; Chen, R.; Shi, H.; Chen, T.; Wang, Z.; Li, H.; Deng, R.; Liu, X.; Huang, W., Stabilizing triplet excited states for ultralong organic phosphorescence. *Nat Mater* **2015**, 14 (7), 685-690.
17. Hirata, S., Recent Advances in Materials with Room-Temperature Phosphorescence: Photophysics for Triplet Exciton Stabilization. *Adv. Opt. Mater.* **2017**, 5 (17), 1700116-n/a.
18. Ma, H.; Peng, Q.; An, Z.; Huang, W.; Shuai, Z., Efficient and Long-Lived Room-Temperature Organic Phosphorescence: Theoretical Descriptors for Molecular Designs. *J. Am. Chem. Soc.* **2019**, 141 (2), 1010-1015.
19. Chen, X.; Xu, C.; Wang, T.; Zhou, C.; Du, J.; Wang, Z.; Xu, H.; Xie, T.; Bi, G.; Jiang, J.; Zhang, X.; Demas, J. N.; Trindle, C. O.; Luo, Y.; Zhang, G., Versatile Room-Temperature-Phosphorescent Materials Prepared from N-Substituted Naphthalimides: Emission Enhancement and Chemical Conjugation. *Angew. Chem. Int. Ed.* **2016**, 55 (34), 9872-9876.
20. Lucenti, E.; Forni, A.; Botta, C.; Carlucci, L.; Giannini, C.; Marinotto, D.; Pavanello, A.; Previtali, A.; Righetto, S.; Cariati, E., Cyclic Triimidazole Derivatives: Intriguing Examples of Multiple Emissions and Ultralong Phosphorescence at Room Temperature. *Angew Chem Int Ed* **2017**, 56 (51), 16302-16307.
21. Lucenti, E.; Forni, A.; Botta, C.; Carlucci, L.; Giannini, C.; Marinotto, D.; Previtali, A.; Righetto, S.; Cariati, E., H-Aggregates Granting Crystallization-Induced Emissive Behavior and Ultralong Phosphorescence from a Pure Organic Molecule. *J. Phys. Chem. Lett.* **2017**, 8 (8), 1894-1898.
22. Xie, Y.; Ge, Y.; Peng, Q.; Li, C.; Li, Q.; Li, Z., How the Molecular Packing Affects the Room Temperature Phosphorescence in Pure Organic Compounds: Ingenious Molecular Design, Detailed Crystal Analysis, and Rational Theoretical Calculations. *Adv. Mater.* **2017**, 29 (17), 1606829-n/a.

23. Bian, L.; Shi, H.; Wang, X.; Ling, K.; Ma, H.; Li, M.; Cheng, Z.; Ma, C.; Cai, S.; Wu, Q.; Gan, N.; Xu, X.; An, Z.; Huang, W., Simultaneously Enhancing Efficiency and Lifetime of Ultralong Organic Phosphorescence Materials by Molecular Self-Assembly. *J. Am. Chem. Soc.* **2018**, *140* (34), 10734-10739.
24. Gu, L.; Shi, H.; Miao, C.; Wu, Q.; Cheng, Z.; Cai, S.; Gu, M.; Ma, C.; Yao, W.; Gao, Y.; An, Z.; Huang, W., Prolonging the lifetime of ultralong organic phosphorescence through dihydrogen bonding. *J. Mater. Chem. C* **2018**.
25. Huang, R.; Ward, J. S.; Kukhta, N. A.; Avó, J.; Gibson, J.; Penfold, T.; Lima, J. C.; Batsanov, A. S.; Berberan-Santos, M. N.; Bryce, M. R.; Dias, F. B., The influence of molecular conformation on the photophysics of organic room temperature phosphorescent luminophores. *J. Mater. Chem. C* **2018**, *6* (34), 9238-9247.
26. Mu, Y.; Yang, Z.; Chen, J.; Yang, Z.; Li, W.; Tan, X.; Mao, Z.; Yu, T.; Zhao, J.; Zheng, S.; Liu, S.; Zhang, Y.; Chi, Z.; Xu, J.; Aldred, M. P., Mechano-induced persistent room-temperature phosphorescence from purely organic molecules. *Chem. Sci.* **2018**.
27. Zhang, Z.; Tang, L.; Fan, X.; Wang, Y.; Zhang, K.; Sun, Q.; Zhang, H.; Xue, S.; Yang, W., N-Alkylcarbazoles: homolog manipulating long-lived room-temperature phosphorescence. *J. Mater. Chem. C* **2018**, *6* (33), 8984-8989.
28. Wang, J.; Chai, Z.; Wang, J.; Wang, C.; Han, M.; Liao, Q.; Huang, A.; Lin, P.; Li, C.; Li, Q.; Li, Z., Mechanoluminescence or Room-Temperature Phosphorescence: Molecular Packing-Dependent Emission Response. *Angew. Chem. Int. Ed.* **2019**, *58* (48), 17297-17302.
29. J. Jacques, A. C., S. H. Wilen, *Enantiomers, Racemates, & Resolutions*. J. Wiley & Sons, New York: 1981.
30. Josse, P.; Favereau, L.; Shen, C.; Dabos-Seignon, S.; Blanchard, P.; Cabanetos, C.; Crassous, J., Enantiopure versus Racemic Naphthalimide End-Capped Helicenic Non-fullerene Electron Acceptors: Impact on Organic Photovoltaics Performance. *Chem. Eur. J.* **2017**, *23* (26), 6277-6281.
31. Hatakeyama, T.; Hashimoto, S.; Oba, T.; Nakamura, M., Azaboradibenzo[6]helicene: Carrier Inversion Induced by Helical Homochirality. *J. Am. Chem. Soc.* **2012**, *134* (48), 19600-19603.
32. Réthoré, C.; Avarvari, N.; Canadell, E.; Auban-Senzier, P.; Fourmigué, M., Chiral Molecular Metals: Syntheses, Structures, and Properties of the AsF₆⁻ Salts of Racemic (±)-, (R)-, and (S)-Tetrathiafulvalene–Oxazoline Derivatives. *J. Am. Chem. Soc.* **2005**, *127* (16), 5748-5749.
33. Pop, F.; Auban-Senzier, P.; Frąckowiak, A.; Ptaszyński, K.; Olejniczak, I.; Wallis, J. D.; Canadell, E.; Avarvari, N., Chirality Driven Metallic versus Semiconducting Behavior in a Complete Series of Radical Cation Salts Based on Dimethyl-Ethylenedithio-Tetrathiafulvalene (DM-EDT-TTF). *J. Am. Chem. Soc.* **2013**, *135* (45), 17176-17186.
34. Brandt, J. R.; Salerno, F.; Fuchter, M. J., The added value of small-molecule chirality in technological applications. *Nat. Rev. Chem.* **2017**, *1* (6), 0045.
35. Yang, Y.; Rice, B.; Shi, X.; Brandt, J. R.; Correa da Costa, R.; Hedley, G. J.; Smilgies, D. M.; Frost, J. M.; Samuel, I. D. W.; Otero-de-la-Roza, A.; Johnson, E. R.; Jelfs, K. E.; Nelson, J.; Campbell, A. J.; Fuchter, M. J., Emergent Properties of an Organic Semiconductor Driven by its Molecular Chirality. *ACS Nano* **2017**, *11* (8), 8329-8338.
36. Rice, B.; LeBlanc, L. M.; Otero-de-la-Roza, A.; Fuchter, M. J.; Johnson, E. R.; Nelson, J.; Jelfs, K. E., A computational exploration of the crystal energy and charge-carrier mobility landscapes of the chiral [6]helicene molecule. *Nanoscale* **2018**, *10* (4), 1865-1876.
37. Chen, W.; Tian, Z.; Li, Y.; Jiang, Y.; Liu, M.; Duan, P., Long-Persistent Circularly Polarized Phosphorescence from Chiral Organic Ionic Crystals. *Chem. Eur. J.* **2018**, *24* (66), 17444-17448.

38. Liang, X.; Liu, T. T.; Yan, Z. P.; Zhou, Y.; Su, J.; Luo, X. F.; Wu, Z. G.; Wang, Y.; Zheng, Y. X.; Zuo, J. L., Organic Room-Temperature Phosphorescence with Strong Circularly Polarized Luminescence Based on Paracyclophanes. *Angew. Chem. Int. Ed.* **2019**, *58* (48), 17220-17225.
39. Hirata, S.; Vacha, M., Circularly Polarized Persistent Room-Temperature Phosphorescence from Metal-Free Chiral Aromatics in Air. *J. Phys. Chem. Lett.* **2016**, *7* (8), 1539-1545.
40. Bouvier, R.; Durand, R.; Favereau, L.; Srebro-Hooper, M.; Dorcet, V.; Roisnel, T.; Vanthuyne, N.; Vesga, Y.; Donnelly, J.; Hernandez, F.; Autschbach, J.; Trolez, Y.; Crassous, J., Helicenes Grafted with 1,1,4,4-Tetracyanobutadiene Moieties: pi-Helical Push-Pull Systems with Strong Electronic Circular Dichroism and Two-Photon Absorption. *Chem. Eur. J.* **2018**, *24* (54), 14484-14494.
41. Dhbaibi, K.; Favereau, L.; Srebro-Hooper, M.; Jean, M.; Vanthuyne, N.; Zinna, F.; Jamoussi, B.; Di Bari, L.; Autschbach, J.; Crassous, J., Exciton coupling in diketopyrrolopyrrole-helicene derivatives leads to red and near-infrared circularly polarized luminescence. *Chem. Sci.* **2018**, *9* (3), 735-742.
42. Li, M.; Li, S. H.; Zhang, D.; Cai, M.; Duan, L.; Fung, M. K.; Chen, C. F., Stable Enantiomers Displaying Thermally Activated Delayed Fluorescence: Efficient OLEDs with Circularly Polarized Electroluminescence. *Angew Chem Int Ed* **2018**, *57* (11), 2889-2893.
43. Gawronski, J.; Kazmierczak, F.; Gawronska, K.; Rychlewska, U.; Nordén, B.; Holmén, A., Excited States of the Phthalimide Chromophore and Their Exciton Couplings: A Tool for Stereochemical Assignments. *J. Am. Chem. Soc.* **1998**, *120* (46), 12083-12091.
44. Gawroński, J.; Brzostowska, M.; Kacprzak, K.; Kołbon, H.; Skowronek, P., Chirality of aromatic bis-imides from their circular dichroism spectra. *Chirality* **2000**, *12* (4), 263-268.
45. Kasha, M.; Rawls, H. R.; El-Bayoumi, M. A., The exciton model in molecular spectroscopy. *Pure Appl. Chem.* **1965**, *11* (3-4), 371-392.
46. Eisfeld, A.; Briggs, J. S., The J- and H-bands of organic dye aggregates. *Chemical Physics* **2006**, *324* (2), 376-384.
47. Wintgens, V.; Valat, P.; Kossanyi, J.; Biczok, L.; Demeter, A.; Bérces, T., Spectroscopic properties of aromatic dicarboximides. Part1.—N—H and N-methyl-substituted naphthalimides. *J. Chem. Soc., Faraday Trans.* **1994**, *90* (3), 411-421.
48. Lakowicz, J. R., *Principles of Fluorescence Spectroscopy*. Springer, New York: 2006.
49. Lower, S. K.; El-Sayed, M. A., The Triplet State and Molecular Electronic Processes in Organic Molecules. *Chem. Rev.* **1966**, *66* (2), 199-241.